Supporting Information

Hosokawa et al. 10.1073/pnas.1006847108

SI Text

Reliability of Our Experimental Results Compared with Cell Force Spectroscopy. Over the past decade, single cell force spectroscopy (SCFS) has been developed and applied to quantify biologically relevant cell-cell adhesions. For example, to quantify leukocyte–endothelial adhesion, a leukocyte immobilized on an AFM cantilever can be attached to endothelial cells cultured on a substrate (adhesion phase). A tensional force can then be loaded by retracting the cantilever, which causes bond rupture and allows measurement of the adhesion (de-adhesion phase). Recently, Ovijit et al. demonstrated that the de-adhesion phase of leukocyte–endothelial adhesion consists of 10 or more major rupture events, each of which corresponds to the rupture of a tether (1). They estimated that the loading force required to rupture one tether was about 100 pN. Using the same cocultures as Ovijit et al., we observed in the present study that an impulse of 2.7×10^{-13} N-s caused an HL-60 leukocyte to slip 1–3 μm on HUVECs.

The natural rolling observed in blood vessels cannot be induced by loading an impulsive force on a leukocyte. This is because the force is not continuous, although it is very strong transiently. Instead, tethers between the leukocyte and HUVECs are ruptured by a slipping (sliding) enforced by the impulsive force. Based on the high-speed imaging data, the time to slip is estimated to be about 1 ms. Although the loading force due to the shockwave should be considered with acoustic impedance mismatching between the medium and object, in our experiment the force due to the jet flow was directly reflected in the targeted objects. In these assumptions, the force causing a leukocyte to slip can be estimated to be 270 pN (2.7×10^{-13} N-s ÷ 1 ms). This suggests that the leukocyte slipping movement observed in Fig. 4*A* included a rupture event of, at most, three tethers. A more detailed observation of how the intercellular breaking progresses spatiotemporally would allow us to more accurately compare our present estimates in the unit of impulse with past estimations in the unit of force.

Single cell force spectroscopy has been used to measure the binding force between single adhesion molecules on living cells (2–7). For example, Panorchan et al. estimated that the single bond force between E-cadherins, which form adherence junctions between epithelial cells, is approximately 100 pN (5). As shown in Fig. 4*B* and Fig. S7*B*, we estimated that when an impulse of approximately 2×10^{-12} N-s was loaded on an MDCK cell–cell interface in two directions (dividing and pushing), the interface was cleaved. Multiple bonds between homophilic or heterophilic pairs of adhesion molecules including E-cadherin, which are formed between two neighboring cell membranes, are generally believed to be ruptured when the two membranes separate 20–40 nm apart from each other (6, 7).

According to our estimates based on high-speed imaging, about 20 μs are required for the neighboring MDCK cell membranes to move 20–40 nm. Therefore, the force causing the MDCK cell–cell interface to separate can be estimated to be 100 nN (2×10^{-12} N-s ÷ 20 μs). This estimate suggests that the interepithelial interface may separate when a force capable of rupturing a thousand E-cadherin bonds is loaded on the interface in two directions. Although the estimate presented here is based on some uncertain assumptions, to our knowledge it is the first reference to the kinetic strength of the overall interepithelial cell adhesion.

Calculation of the Impulse Loaded on the AFM Cantilever. The geometrical relationship between the laser focal point O_f and the AFM cantilever is illustrated in Fig. S1*B*. When an impulse with a magnitude of F_0 [N-s] is generated at O_f $(0, 0, Z_0)$ and propagates spherically as a short wave packet, it decreases with the square of the distance R from O_f. Therefore the impulse on a small fraction of the AFM cantilever can be written as

$$\Delta f(x,y) = -F_0 \frac{\Delta a \cdot \Delta b}{4\pi R^2}. \quad \textbf{[S1]}$$

The small fractions Δa and Δb that are on a sphere with radius R can be converted to fractions on the AFM cantilever, Δx and Δy, by

$$\Delta a = \cos\varphi' \cdot \Delta x = \frac{|Z_0|}{\sqrt{(X_0 + x)^2 + {Z_0}^2}} \Delta x, \quad \textbf{[S2]}$$

$$\Delta b = \cos\varphi'' \cdot \Delta y = \frac{|Z_0|}{\sqrt{y^2 + Z_0^2}} \Delta y. \quad \textbf{[S3]}$$

The impulse that pushes the cantilever—i.e., the Z-direction component of Δf—is expressed as

$$\Delta f_Z(x,y) = \Delta f(x,y) \cos\varphi. \quad \textbf{[S4]}$$

From Eqs. **S1**, **S2**, and **S3**, Eq. **S4** is rewritten as

$$\Delta f_Z(x,y) = -\frac{F_0}{4\pi} \cdot \frac{{Z_0}^3}{\{(X_0 + x)^2 + y^2 + {Z_0}^2\}^{3/2}} \cdot \frac{\Delta x}{\sqrt{(X_0 + x)^2 + {Z_0}^2}} \cdot \frac{\Delta y}{\sqrt{y^2 + {Z_0}^2}}. \quad \textbf{[S5]}$$

When the slope of the AFM cantilever with angle of θ is considered (as shown in Fig. S1*C*), the coordinate system is rotated as

$$\Delta f_Z(x,y) = -\frac{F_0}{4\pi} \cdot \frac{{Z'_0}^3}{\{(X'_0 + x)^2 + y^2 + {Z'_0}^2\}^{3/2}} \cdot \frac{\Delta x}{\sqrt{(X'_0 + x)^2 + {Z'_0}^2}} \cdot \frac{\Delta y}{\sqrt{y^2 + {Z'_0}^2}} \quad \textbf{[S6]}$$

where $\begin{pmatrix} X'_0 \\ Z'_0 \end{pmatrix} = \begin{pmatrix} \cos\theta & -\sin\theta \\ \sin\theta & \cos\theta \end{pmatrix} \begin{pmatrix} X_0 \\ Z_0 \end{pmatrix}$.

Eq. **S6** corresponds to Eq. **2**. The total impulse loaded on the cantilever is expressed as

$$F^0_{\mathrm{AFM}} = \iint_S f_Z(x,y)\,dx\,dy \quad \textbf{[S7]}$$

where S is the area of the AFM cantilever.

Calculation of the Impulse Loaded on a Sphere. When an impulse of magnitude F_0 is generated at O_f and propagates spherically as a short wave packet to a sphere as shown in Fig. S4*D*, the direction of the impulse loaded on the sphere is indicated as a vector from O_f to the center of the sphere O_{sph}. This is because the impulse perpendicular to the vector is canceled by the symmetry. Therefore, the impulse f loaded on the sphere is expressed as

$$f = F_0 \frac{\int_0^{r_D} 2\pi {r_D}' \cos\theta' d{r_D}'}{4\pi R^2} \quad \textbf{[S8]}$$

where ${r_D}'$ and θ' are the distance and angle between O_{sph} and a

point on a sphere with radius of R, corresponding to the distance between O_f and O_{sph}. The $r_D{}'$ is expressed as a function of θ':

$$r_D{}' = 2R\sin\frac{\theta'}{2}. \quad \textbf{[S9]}$$

The $r_D{}'$ on tangential line of the sphere is expressed as

$$r_D = 2R\sin\frac{\theta}{2}. \quad \textbf{[S10]}$$

From Eqs. **S9** and **S10**, Eq. **S8** is solved as

$$f = \frac{F_0}{4}\sin^2\theta. \quad \textbf{[S11]}$$

Furthermore, when the relations:

$$\sin\theta = \frac{r}{R} \quad \text{and} \quad R^2 = X^2 + Z^2 \quad \textbf{[S12]}$$

are taken into consideration, the impulse is given by

$$f = F_0\frac{r^2}{4(X^2+Z^2)}. \quad \textbf{[S13]}$$

When the laser is focused at ventral side of the sphere ($Z = 0$), the impulse is expressed as

$$f(x) = \frac{F_0}{4}\cdot\left(\frac{r}{x}\right)^2, \quad \textbf{[S14]}$$

which corresponds to Eq. **3**.

Estimation of the Impulse Loaded on the Front Surface of the MDCK Cell Layer. The interface surface between the cell layer and cell-free area is treated as a sequential flat plane (Fig. S7*A*). When an impulse of magnitude F_0 propagates spherically, the impulse loaded on a small fraction on the plane is written as

$$\Delta f(R,y) = F_0\frac{\Delta a\cdot\Delta b}{4\pi R^2}, \quad \textbf{[S15]}$$

where R is the distance between the laser focal point and the center of the plane. The small fractions Δa and Δb are on the sphere with a radius R. When Δa is very small, it corresponds to the horizontal width of the plane. The Δa is expressed as an angle function of $\Delta\theta$ at O_f:

$$\Delta a = 2R\tan\left(\frac{\Delta\theta}{2}\right). \quad \textbf{[S16]}$$

The fraction Δb can be converted to the fraction Δz on the plate in the direction of the layer thickness (Z-direction in the figure):

$$\Delta b = \cos\varphi\cdot\Delta z = \frac{R}{\sqrt{R^2+z^2}}\Delta z. \quad \textbf{[S17]}$$

When O_f is at the center of the layer in the Z-direction, the direction of the impulse loaded on the plane is parallel to the R-direction. This is because the vector component of the impulse parallel to the Z-direction is cancelled by the symmetry. Hence, we extract the vector component parallel to the R-direction Δf_R:

$$\Delta f_R(R,z) = \Delta f(R,z)\cos\varphi. \quad \textbf{[S18]}$$

From Eqs. **S15**, **16**, and **S17**, Eq. **S18** is rewritten as

$$\Delta f_R(R,z) = \frac{F_0}{2\pi}\tan\left(\frac{\Delta\theta}{2}\right)\cdot\frac{R}{R^2+z^2}\Delta z. \quad \textbf{[S19]}$$

Therefore, the impulse loaded on the plane is solved as

$$f_R(R) = 2\int_0^{D/2}\frac{F_0}{2\pi}\tan\left(\frac{\Delta\theta}{2}\right)\cdot\frac{R}{R^2+z^2}dz = \frac{F_0}{\pi}\tan\left(\frac{\Delta\theta}{2}\right)\cdot\tan^{-1}\frac{D}{2R}, \quad \textbf{[S20]}$$

where D is the layer thickness.

The interface surface between the cell layer and the cell-free area is divided into flat planes as a function of $\Delta\theta$. f_R is calculated for each plane. When the origin of the angle θ at O_f is in the direction from O_f to the cleaved interface (bottom graphic in Fig. 4*B* and Fig. S7*B*), the impulse to push the cleaved cell–cell interface, corresponding to red gradation in top graphic of Fig. 4*B* and Fig. S7*B*, is expressed as

$$f_{\text{red}}(R,\theta) = f_R(R)\cdot\cos\theta. \quad \textbf{[S21]}$$

Simultaneously, the impulse to divide the cleaved cell–cell interface, corresponding to the green and blue gradations in top graphic of Fig. 4*B* and Fig. S7*B*, is

$$f_{\text{Green and Blue}}(R,\theta) = f_R(R)\cdot\sin\theta. \quad \textbf{[S22]}$$

The arrows in top graphic of Fig. 4*B* and Fig. S7*B* are the integrals of Eq. **S21** or Eq. **S22** with respect of θ. The gradations are calculated by fixing $\Delta\theta$ on 1 degree. The calculation is also performed with a $\Delta\theta$ of 0.5 or 2 degrees. Because the distribution of the gradations and their integrals hardly depend on $\Delta\theta$, we judge that our calculation algorithm made by Visual Basic 6.0 (Microsoft) is reliable.

The impulse estimation was performed at seven interfaces between MDCK cells selected randomly from independent cultures (Table S1). The result of Case 1 together with the cell microphotograph is shown in Fig. 4*B*, and those of Cases 2 and 3 are shown in Fig. S7*B*.

Mean Impulse to Detach Cell Pair. When the distribution of the intercellular breaking force of two-cell NIH3T3 fibroblast aggregates is approximated as a Gaussian distribution (Fig. S8*A*), the provability distribution of cell detachment is written as

$$P(F) = \frac{1}{\sigma\sqrt{2\pi}}\int_{-\infty}^{F}\exp\left(-\frac{(f-F_{\text{mean}})^2}{2\sigma^2}\right)df, \quad \textbf{[S23]}$$

where F and F_{mean} are the impulse loaded on the two-cell aggregate and mean impulse to detach the cell pair, respectively. The standard score at the impulse F is expressed as

$$z = \frac{F-F_{\text{mean}}}{\sigma}. \quad \textbf{[S24]}$$

When we confirm two probabilities (P_1 and P_2) of cell detachment under impulses of F_1 and F_2 from the experiments, the standard scores (z_1 and z_2) are defined as an inverse function of

$$P_n(z_n) = \frac{1}{\sqrt{2\pi}}\int_{-\infty}^{z_n}\exp\left(-\frac{z'^2}{2}\right)dz'. \quad \textbf{[S25]}$$

Therefore, mean impulse is estimated as

$$F_{\text{mean}} = F_1 - z_1(P_1)\cdot\sigma \quad \textbf{[S26]}$$

with a standard deviation of

$$\sigma = \frac{F_1 - F_2}{z_1(P_1) - z_2(P_2)}. \qquad \textbf{[S27]}$$

The standard score z_1 is estimated from the percentage of cell detachment shown in Fig. 2*B*. Under the experimental condition, the impulse F_0 at O_f was estimated to be 42×10^{-12} N-s (Fig. S2*E*). From Eq. **S14** and the geometrical relationship between O_f and the two-cell aggregate (Fig. S8*B*), the impulse to dissociate the cell pair is estimated as

$$F_1 = f_1(r_1) + f_2(r_2) = \frac{1}{2}F_0 = 21 \times 10^{-12}\ [\mathrm{N-s}]. \qquad \textbf{[S28]}$$

To estimate the standard deviation σ, we investigated the percentage of homotypic two-cell aggregates that expressed the isoform c when the laser had a pulse energy of 160 nJ/pulse. Under this experimental condition, the percentage (P_2) and total impulse F_2 were 30% and 10×10^{-12} N-s, respectively. From these results and Eq. **S27**, σ was estimated to be 7.5×10^{-12} N-s. The mean impulse, except for the homotypic two-cell aggregate expressing isoform c, was also estimated by Eq. **S26** using σ, assuming that the standard deviation is hardly varied by the combination of isoforms.

The mean impulse to dissociate two-cell aggregates ranged 1.2 to 1.7×10^{-11} N-s (Fig. S8*C*). This estimate would be disturbed by the following possibilities: (*i*) The laser focus is diffused by the cell, and/or (*ii*) the direct laser ablation of the cell contributes to the detachment. However, in our experience, the order of the impulse in which a whole cell is detached from another cell is reliable compared to that of the rupture of a leukocyte (2.6 to 2.8×10^{-13} N-s). Thus, these negative possibilities could be neglected in our rough estimation.

1. Ovijit C, Sapun HP, Wilbur AL, Daniel AF (2009) Combined atomic force microscopy and side-view optical imaging for mechanical studies of cells. *Nat Methods* 6:383–387.
2. Helenius J, Heisenberg CP, Gaub HE, Muller DJ (2008) Single-cell force spectroscopy. *J Cell Sci* 121:1785–1791.
3. Bajpai S, Feng Y, Krishnamurthy R, Longmore GD, Wirtz D (2009) Loss of alpha-catenin decreases the strength of single E-cadherin bonds between human cancer cells. *J Biol Chem* 284:18252–18259.
4. Dobrowsky TM, Panorchan P, Konstantopoulos K, Wirtz D (2008) Chapter 15: Live-cell single-molecule force spectroscopy. *Method Cell Biol* 89:411–432.
5. Panorchan P, et al. (2006) Single-molecule analysis of cadherin-mediated cell-cell adhesion. *J Cell Sci* 119:66–74.
6. Franz CM, Taubenberger A, Puech PH Muller DJ (2007) Studying integrin-mediated cell adhesion at the single-molecule level using AFM force spectroscopy. *Sci STKE* 406:l5.
7. Waschke J, et al. (2007) Imaging and force spectroscopy on desmoglein 1 using atomic force microscopy reveal multivalent $Ca^{(2+)}$-dependent, low-affinity trans-interaction. *J Membrane Biol.* 216:83–92.

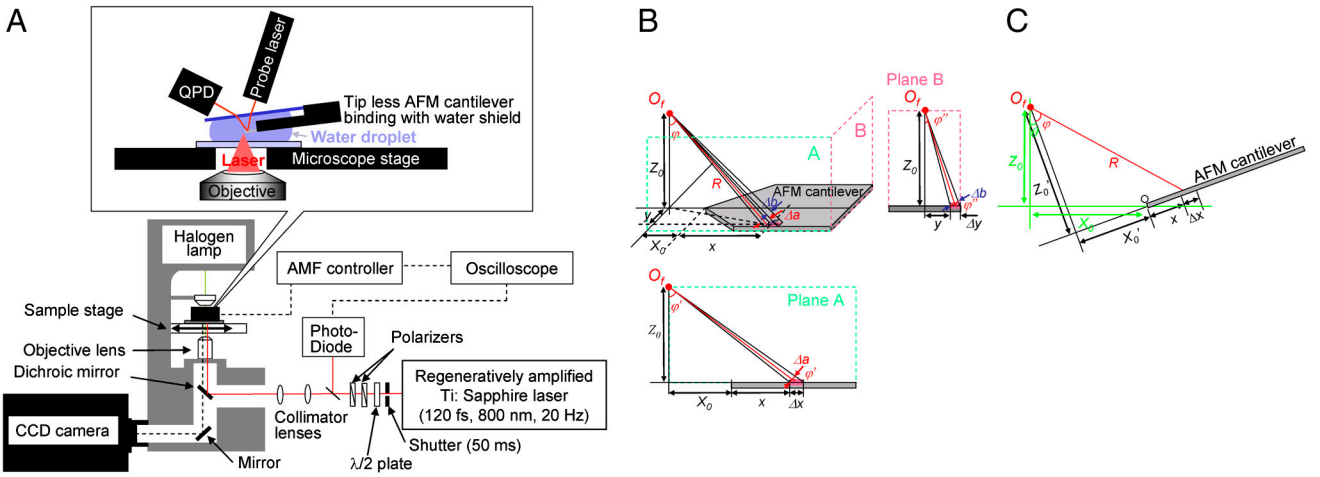

Fig. S1. (*A*) Experimental setup of the AFM-assisted impulse measurement system and the femtosecond laser system. (*B* and *C*) Geometrical relationship between the laser focal point O_f and AFM cantilever.

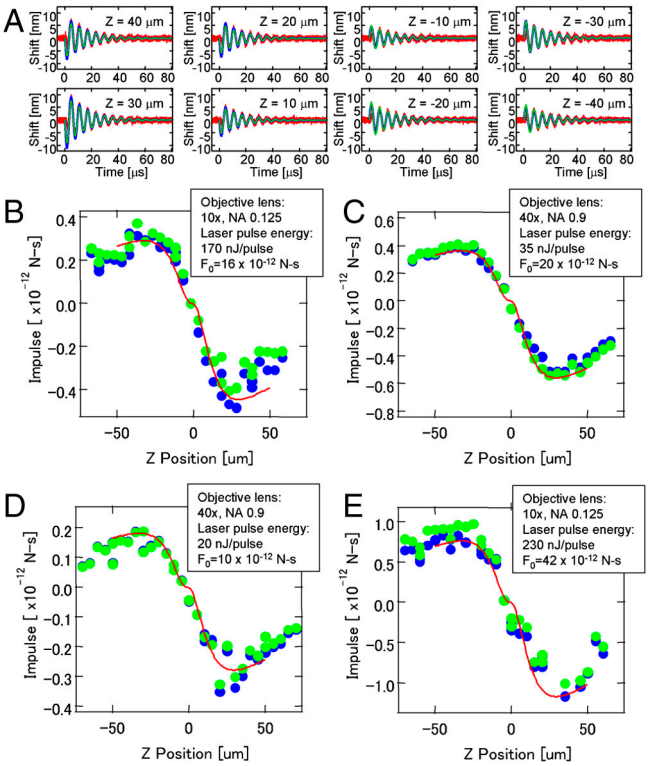

Fig. S2. (*A*) Z-position dependence of the transient oscillation of the AFM cantilever on the experimental condition presented in Fig. 1. Blue lines are the least-square fitting using Eq. **1**, where the impulse F, angular velocity ω, and damping constant α were treated as variable parameters. Green lines are the fitted results where the oscillation frequency ($\omega/2\pi$) and damping time ($1/\alpha$) were fixed at 160 [Hz] and 17 [μs], respectively, and impulse F was treated as the only variable parameter. All observed data were well-reproduced by Eq. **1**. (*B–E*) *Z*-position dependence of impulse F on the AFM cantilever corresponding to the results of (*B*) Fig. 1, (*C*) Fig. 4*A*, (*D*) Fig 4*B*, and (*E*) Fig. 2. Blue dots were determined using least-square fitting in which the impulse F, angular velocity ω, and damping constant α were variable parameters. Green dots were the fitted results when impulse F was the only variable parameter. All observation data were well-reproduced by Eq. **1**, as were those shown in *A*. Red lines were calculated by Eq. **2**, in which F_0 was the only variable parameter.

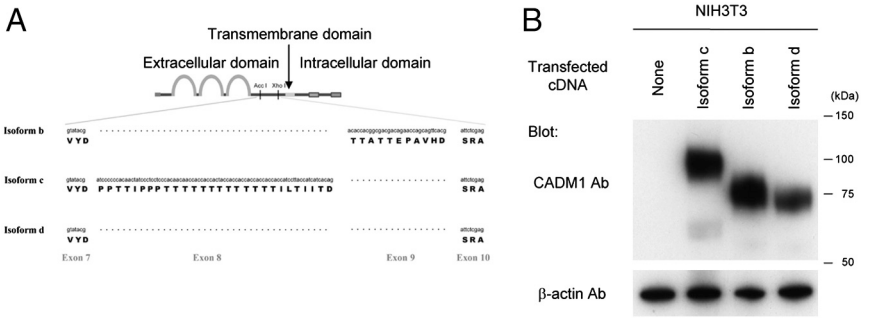

Fig. S3. (*A*) Nucleotide sequence proper to individual CADM1 isoforms. The nucleotide sequences of the coding regions of the CADM1 isoform cDNAs are shown between the AccI and XhoI sites, along with their deduced amino acid sequences. The AccI-XhoI regions are present between the third Ig-like domain and the transmembrane domain of CADM1, as illustrated above. (*B*) Western blot analyses of CADM1 isoforms in NIH3T3 subclones. Cell lysates were prepared from NIH3T3 cells and subclones transfected with the CADM1 isoform cDNAs indicated, and were blotted with an antibody against the CADM1 C-terminus. After stripping, the blot was reprobed with an anti-β-actin antibody as a loading control.

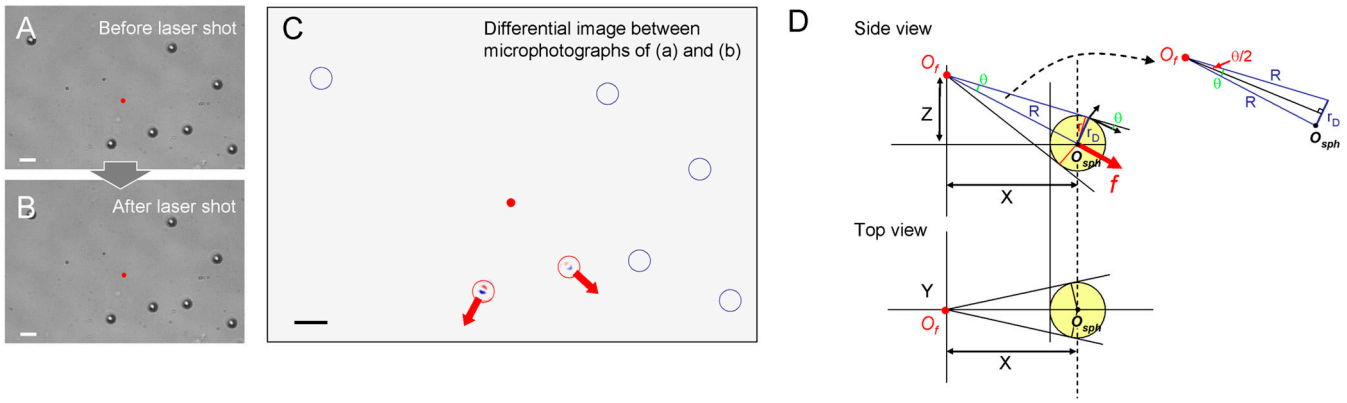

Fig. S4. (*A*–*C*) Microphotographs of streptavidin-coated microspheres adhering to a biotin-coated substrate before (*A*) and after (*B*) a laser shot, and the differential image (*C*) between *A* and *B*. Blue and red contrasts in *C* indicate the degree to which the brightness is increased and decreased, respectively. These contrasts are clearly shown for microspheres in red circles in *C*, although there are no contrasts for residual microspheres in blue circles. This means that microspheres in red circles are moved by the impulsive force at the direction indicated by red arrows in *C*. Bar = 10 μm. Red dot indicates the laser focal point. (*D*) Geometrical relationship between the laser focal point O_f and the sphere.

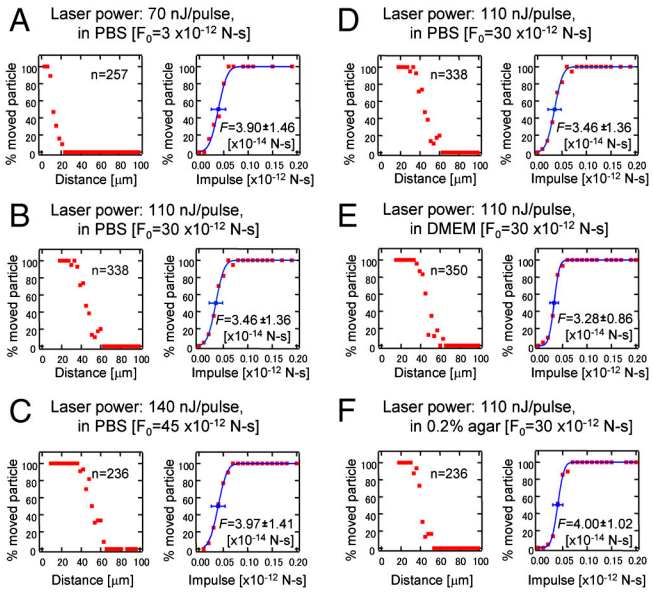

Fig. S5. Movement of biotin-adhering streptavidin-coated microspheres when a femtosecond laser with a pulse energy of 70 (*A*), 110 (*B*), or 140 (*C*) nJ/pulse was focused into the PBS medium and when a femtosecond laser with pulse energy of 110 nJ/pulse was focused into a medium of PBS (*D*), DMEM (*E*), or 0.2% bactoagar (*F*). Left and right graphs display the percentage of particles that moved vs. the distance between the laser focal point and the sphere center (left), or vs. the impulse estimated by Eq. **3** (right). Blue lines in the graphs to the right are least-square fittings of Eq. **4**. Blue box and error bar on the line indicate *F* and δF in the function, respectively, corresponding to the estimated mean impulse and its standard deviation to move particles.

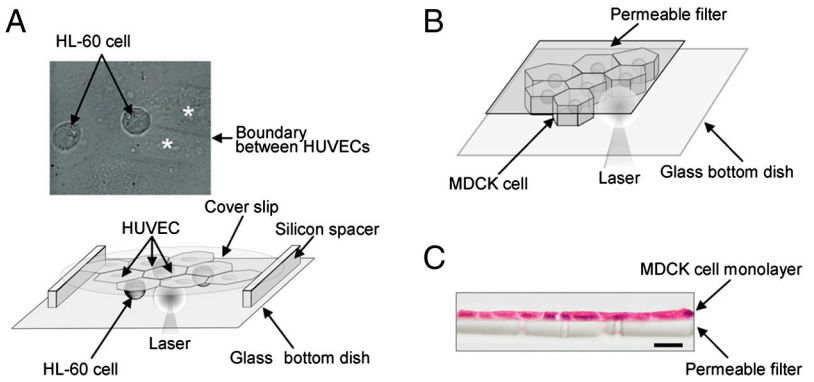

Fig. S6. (*A*) Schematic presentation of how the femtosecond laser was focused on leukocyte–endothelial cocultures. An HL-60 leukocyte–HUVEC coculture was established on a cover slip (*Upper*, phase contrast image), which was placed cell-adherent side down on an automated stage of an inverted microscope equipped with a femtosecond laser (*Lower*). The laser was focused through an objective lens at a position a few microns below the filter. Asterisks indicate nuclei of HUVECs. (*B*) Schematic presentation of how the femtosecond laser was focused on MDCK cell cultures. The MDCK epithelial monolayer was established on a permeable filter, which was placed cell-adherent side down on an automated stage of an inverted microscope equipped with a femtosecond laser. The femtosecond laser was focused through an objective lens at a position a few microns below the filters. (*C*) Histological examination of MDCK cell cultures. MDCK cell cultures on permeable filters were fixed with formalin, embedded in paraffin, and cut into sections. Sections were stained with hematoxylin and eosin and observed through a microscope. Bar = 20 μm.

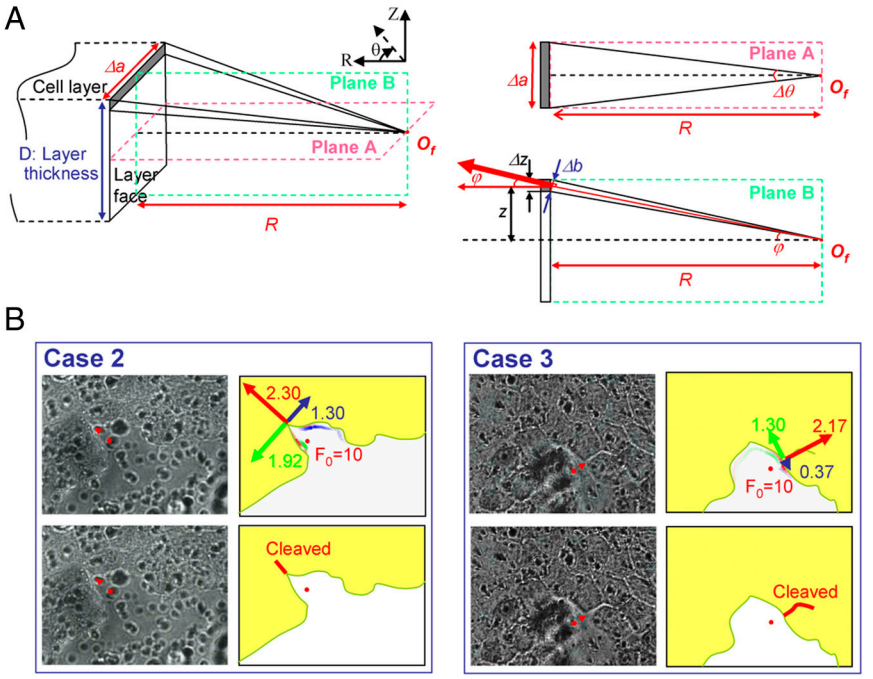

Fig. S7. (*A*) Geometrical relationship between the laser focal point O_f and interface surface between the MDCK cell layer and the cell-free area. (*B*) Representative results of the femtosecond laser-induced cleavage of the MDCK cell–cell interface, with the exception of that shown in Fig. 4*B*. The experimental condition and the figure arrangement of each result correspond to those of Fig. 4*B*.

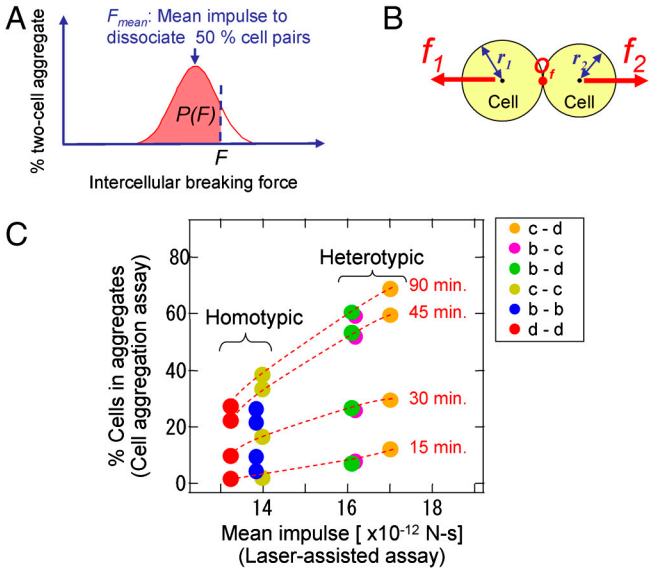

Fig. S8. (*A*) Explanation of the distribution of two-cell aggregates as a function of intercellular breaking force. A Gaussian distribution was assumed to reflect the distribution of the individual intercellular breaking forces of each cell pair. (*B*) Geometrical relationship between the laser focal point O_f and the two-cell aggregate. (*C*) Relationship between the mean impulse evaluated by the laser-induced impulsive force and the percentage of cell aggregates, as generated by the cell aggregation assay. Mean impulses were plotted instead of the % success of cell dissociation in Fig. 2*C*.

Table S1. Impulses to push and to divide the cell–cell interface of the MDCK cell layer

Case	Impulse to push (Red)	Impulse to divide (Blue + Green)
1	1.39	0.80 + 0.59
2	2.30	1.30 + 1.92
3	2.17	0.37 + 1.30
4	2.10	0.97 + 1.51
5	1.80	0.86 + 1.20
6	1.75	1.27 + 0.52
7	1.43	0.68 + 1.29
Mean	1.85	2.08
Standard deviation	0.36	0.61